User Aligned Histogram Stacks for Visualization of Abdominal Organs via MRI

M Özdemir[1], O Akay[2], C Güzeliş[3], O Dicle[4], M A Selver[2]

[1]Institute of Natural and Applied Sciences, Dokuz Eylul University, Kaynaklar Campus, 35160, Buca, Izmir, TURKEY

[1]Department of Electrical and Electronics Engineering, Dokuz Eylul University, Kaynaklar Campus, 35160, Buca, Izmir, TURKEY

[2]Department of Electrical and Electronics Engineering, Yaşar University, Selçuk Campus, 35320, Bornova, İzmir, TURKEY

[1]Department of Radiology, Faculty of Medicine, Dokuz Eylul University, Balçova, Izmir, TURKEY

Email merveozdemir89@gmail.com, olcay.akay@deu.edu.tr, oguz.dicle@deu.edu.tr, cuneyt.guzelis@yasar.edu.tr , alper.selver@deu.edu.tr,

Abstract. Multi-dimensional transfer functions (MDTF) are occasionally designed as two-step approaches. At the first step, the constructed domain is modelled coarsely using global volume statistics and an initial transfer function (TF) is designed. Then, a finer classification is performed using local information to refine the TF design. In this study, both a new TF domain and a novel two-step MDTF strategy are proposed for visualization of abdominal organs. The proposed domain is generated by aligning the histograms of the slices, which are reconstructed based on user aligned majority axis/regions through an interactive Multi-Planar Reconstruction graphical user interface. It is shown that these user aligned histogram stacks (UAHS) exploit more a priori information by providing tissue specific inter-slice spatial domain knowledge. For initial TF design, UAHS are approximated using a multi-scale hierarchical Gaussian mixture model, which is designed to work in quasi real time. Then, a finer classification step is carried out for refinement of the initial result. Applications to several MRI data sets acquired with various sequences demonstrate improved visualization of abdomen.

1. Introduction

Visualization of abdominal organs (kidneys, liver, and spleen) plays critical role in several clinical procedures including but not limited to surgery planning, treatment follow-ups, and education. Although there are many segmentation techniques developed for abdomen, they mostly rely on explicit classification of the voxels belonging to the organ of interest ignoring the rest of the data. However, in most of the cases, what is interesting from the clinical point of view is not only an organ or tissue itself, but also its relationships with the neighboring organs and/or vessel systems. Thus, even if the segmentation is perfectly realized, it is not possible to render it together with the adjacent tissues/organs and related vascular trees unless another segmentation process is performed for each object of interest [1].

This limitation of segmentation motivates the development of complicated TF specification techniques which allow enhancement of potentially important features during the rendering. In other words, TF design provides suppression of the redundant data, while facilitating intervention of physician for further modifications over the complete volume. Moreover, TF design is the only interactive step of the direct volume rendering pipeline and intuitive design user interfaces allow production of informative renderings [2].

TFs map data attributes (i.e. domain) to visual properties (i.e. range) such as color and opacity. In medical applications, domain should utilize enough features for discrimination of different tissues/organs. At the same time, complexity of user interaction and input dimensionality need to be considered carefully in order to preserve intuitiveness and better computational performance. In other words, tissues are usually indistinctive in low dimensional domains and the interactions become counterintuitive or infeasible in high dimensional ones. This trade-off between preserving intuitive user interaction and possessing a discriminative domain spurs ongoing research efforts in TF design.

There are three main approaches of TF design: Manual [3], image-centric [9-12], and data-centric. Data-centric methods have been gaining more importance since they increase the classification capabilities of TFs. In this manner, iso-value determination [4], edge detection concepts [5], topology analysis [6], stochastic properties [7], texture characteristics and 3-D filter responses [13] are some of the proposed effective techniques. Various graphical user interfaces (GUIs) [15] and interaction mechanisms [16-17] have also been developed using multi-dimensional transfer functions (MDTF) [18-19].

For medical visualization, recent studies show that incorporating medical domain knowledge through semantic expressions, anatomical/physiological information, and/or modality characteristics allow obtaining accurate renderings with a TF specification [20].

The method proposed in this study shares the same strategy (i.e. coarse classification plus refinement) with the above discussed MDTF techniques. Compared to those, our method performs further steps on TF specification in the following aspects: First of all, a new and very intuitive TF domain is constructed by histogram stacks, which are calculated from reconstructed images (i.e. resampled volume data) based on user aligned majority axis through an Multi-Planar Reconstruction (MPR) user interface (Section 3). Secondly, a multi-scale hierarchical Gaussian Mixture Model (GMM) strategy, which is able to locate and roughly classify tissue of interest automatically and in (quasi) real time, is developed (Section 4). Thirdly, refinement of classification results based on spatial and morphological relations of the tissues of interest are performed. Finally, the developed approach is tested using various clinical abdominal MRI data sets with different sequence protocols (Section 5).

2. Data Sets

The analyses in this study are applied to several MRI series, which are obtained by the Radiology Department of Dokuz Eylül University. The data sets are acquired using a 1,5T Philips MRI modality that produces 12 bit DICOM images with a resolution of 256 x 256. The data sets were retrospectively collected from the Picture Archiving and Communication System of the same department. Three different MRI sequences (i.e. T1-DUAL (in-phase), THRIVE, T1-WATS) are used to test the proposed method. Each of these sequences is routinely being used to scan the same part of the body, but they are obtained from different combinations of radiofrequency pulses and gradients [23]. The details of the characteristics of these data sets and the utilized sequences are given below and their sample images are illustrated in Figure 1.

T1-DUAL (in phase) is a fat suppression sequence which uses the time differences in the z-axis recoveries of fat and water protons. The signal is acquired twice: first, when water and fat protons are in phase; and second, when they are out of phase (while excited protons are returning to their first position). By choosing the suitable time of echo, fat suppression can be accomplished by subtracting corresponding frequencies of fat and water signals. Thus, this sequence is very useful to understand the fat content. Being T1-weighted, T1-DUAL is very effective to identify blood and tissues that are rich in protein and helps in determining the lubrication levels. In this study, 14 data sets, which have

ISDs that vary between 5.5 mm and 9 mm (average 7.84 mm), x/y spacing is between 1.44 - 1.89 mm (average 1.61 mm) and the number of slices between 26 and 50 (average 36), are used. THRIVE is a fast imaging sequence that is obtained by scanning the liver consecutively in a short time with thin slices to obtain the response of a known lesion to a contrast agent. THRIVE provides observation of the signal increase originating from the contrast agent instead of image quality. In total, 7 THRIVE data sets with 2.5 mm of ISD are used. Due to this small ISD, these data sets have slices between 80 and 110 (average 93). Although their ISDs are constant, x-y spacing changes between 1.56 and 1.97 mm (average 1.67 mm). In this study, 5 THRIVE data sets are used. Finally, WATS (WATer Selective) is a high resolution T1-weighted fat suppression sequence. 5 WATS data sets used in this study have x-y spacing between 5.5 - 9 mm (average of 7.9 mm). Their x-y spacing changes between 1.36 - 1.67 mm (average 1.43 mm) and the number of slices vary between 26 and 40 (average 37).

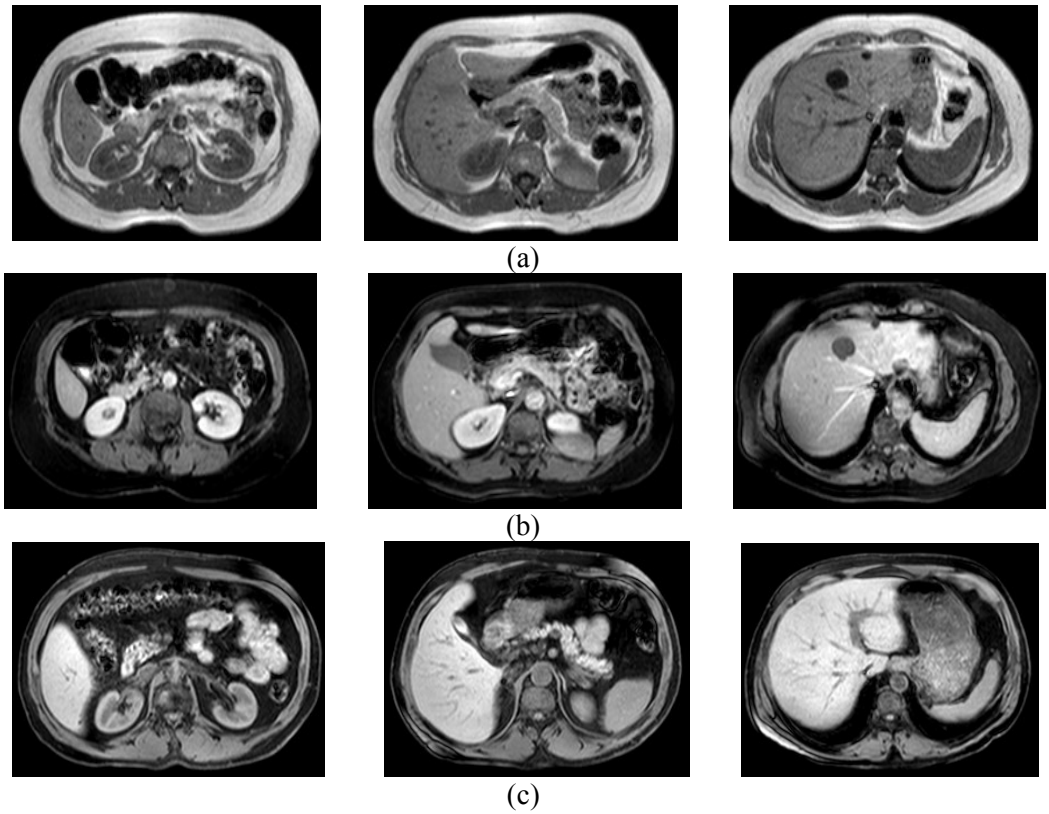

Figure 1. Sample abdominal images from sequences: a) T1-DUAL, b) THRIVE, c) WATS.

3. User Aligned Volume Histogram Stacks

Construction of a User Aligned Histogram Stack (UAHS) is a simple procedure for a physician who uses MPR interfaces and tools during his/her daily workflow. By using the developed MPR interface, the physician determines a majority axis or region for the organ of interest. The majority axis can be a spline or a (piecewise) line and majority region can be an ellipse or a rectangle. The selection of the region or axis should be consistent with the shape and size of the organ of interest. As an example, the geometry of the kidney is elliptical in axial slices. Therefore, applying an elliptical region would be more effective than the others (Fig 2.a-c). As a second example, selecting a rectangular region to reconstruct the liver is not sensible, because its complex size would require a very large area. Thus, a spline based majority axis is better suited to represent the liver (red line in Fig 2.h).

After this selection is done on a single MPR plane (axial, sagittal, or coronal), one of the remaining MPR planes is used to determine the slices, where the organ of interest is visible. This is a very simple

interaction that only needs the user to draw a line over the organ of interest (see Fig 2.b for the kidney and Fig 2.a or 2.b for the liver).

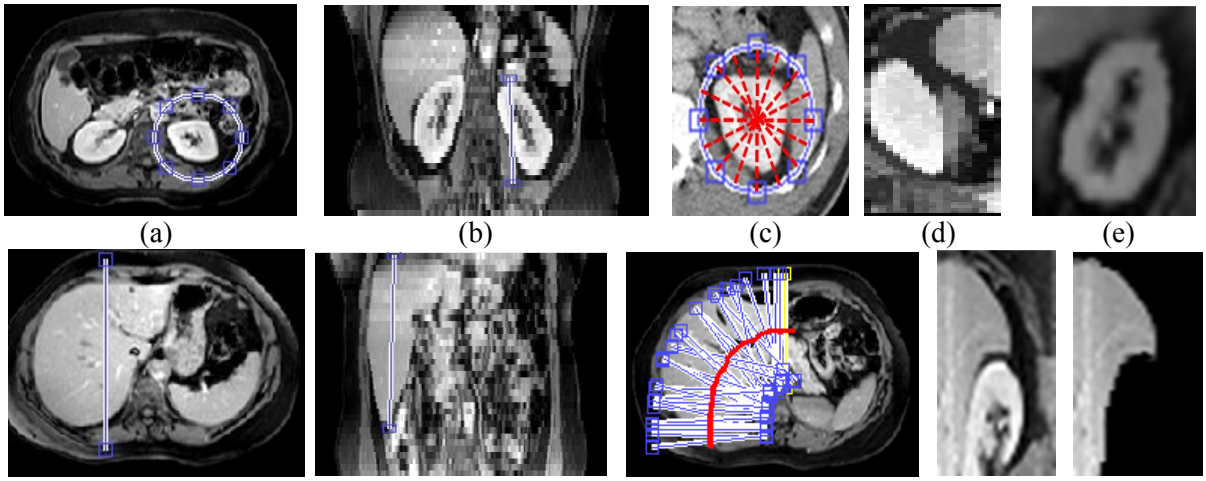

Figure 2. Scattered signals at 90^{o} and 1.8 cm distance with 10, 0, and -10 dB SNR.

These two interactions are the only ones required for the construction of UAHS. Next, the developed software generates new reconstructed images using these user inserted planes and by dividing the selected areas into new sampling planes (See Fig 2.d and 2.e for the kidney and Fig 2.i and 2.j for the liver). By aligning the histograms of each reconstructed image (Fig. 3), UAHS, which provides a new data representing the object of interest in a more focused way, is obtained (Fig. 4).

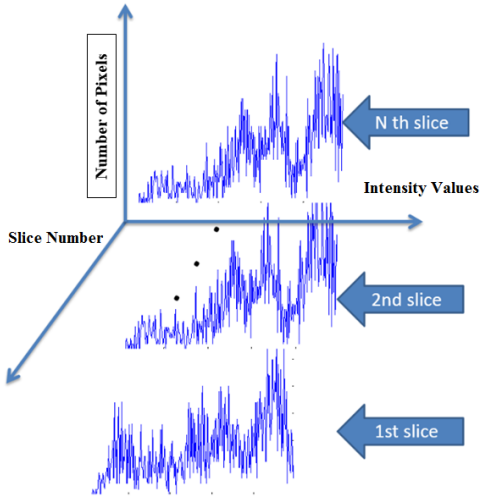

Figure 3. Aligning the histograms of the reconstructed image slices.

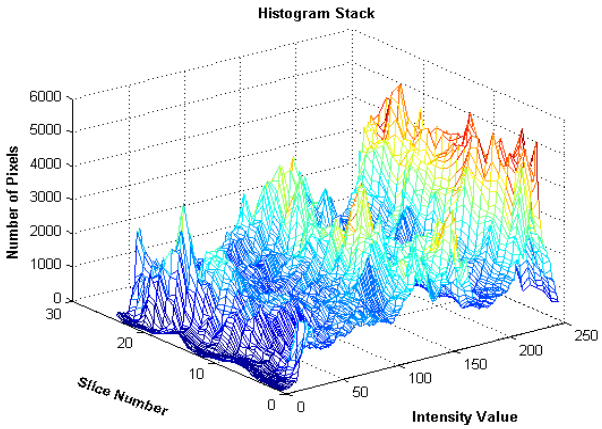

Figure 4. An example of UAHS.

4. Approximation of UAHS via Gaussian Functions

The gray values for organs of interest have varying intensity ranges and characteristics even for the same organ in different MRI acquisitions. However, by evaluating UAHS with respect to different MR sequences, some common characteristic properties are observed in UAHS. One of them is that UAHS becomes narrower at the beginning or end slices and widens in the middle slices. It should be noted

that the use of DICOM image series, which supply large numbers of gray levels, is necessary to obtain a compact desired histogram. The other important point is that the desired histogram should be distinguishable from the unwanted components/tissues. This distinction in UAHS generates two valleys in both sides of the UAHS. Figure 5 illustrates three examples of UAHS data, which are obtained using the developed GUI and for liver visualization, along with their desired counterparts.

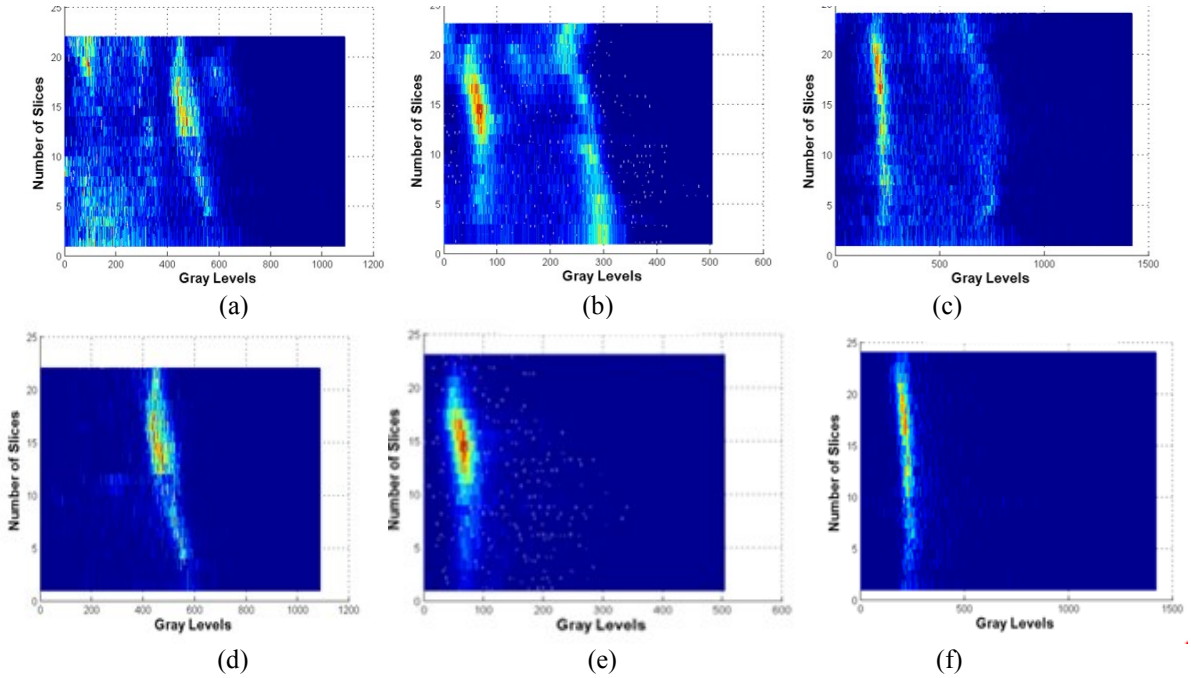

Figure 5. (a)-(c) Top view of resultant UAHS of the GUI constructed for liver visualization from different MRI sequences, (d)-(f) Top view of their respective desired counterparts.

The UAHS should be modeled in order to determine the valleys in a robust manner. Thus, the selection of the lobes from the UAHS requires an approximation to obtain the desired lobes. For modeling a UAHS, some important issues must be taken into account. One of them is the non-smooth structure of UAHS because of the intensity fluctuations of MRI. The second problem is the variability in the gray level range of the same organ among slices. The third problem is the slice thickness of the MRI data that causes a limited sampling in z-direction and results in a high inter-slice distance.

The shape of the UAHS is like a bell curve with a certain radius and intensity. In the center of the UAHS, there exist a lot of pixels that create high amplitude bells, each of which is called a “lobe”. Gaussian function is a good approximation for fitting the lobes of UAHS. Besides, defining the UAHS in terms of Gaussian functions provides an intuitive initial TF design employing the parameters of Gaussian function. Various possible Gaussian basis functions can be created as a filter bank employing multiple orientation and scale values.

In this study, by considering the above mentioned criteria, a hierarchical and multi-scale modeling is proposed. In an iterative manner, the proposed model tries to find the best Gaussian basis to fit the corresponding lobe of the UAHS. The developed algorithm provides a procedure for capturing all the suppressed lobes of importance in a successive manner by associating the lobes with a suitable number of Gaussian basis functions.

Using different scales provides the user with the convenience of expressing different lobes in the right way. However, the characteristics of UAHS demonstrate that lobes can have curvy structures. The best approximation for these curvy parts is to integrate the rotation parameter to the algorithm as an extra degree of freedom. For a fixed scale parameter, the best rotation parameter is determined through the calculation of correlation between the Gaussian basis functions and UAHS. Correlation

can be calculated in an easier way in the frequency domain by multiplying the Fourier transform of the UAHS by the conjugate of the Fourier transform of the Gaussian basis function.

A rotated and axis scaled Gaussian basis function can be expressed with respect to given a, θ, and ε parameters as follows;

$$g_{a,\theta}(x',y') = e^{-1/2(\varepsilon^{-1}(a^2(x'\cos\theta - y'\sin\theta)^2) + a^2(x'\sin\theta - y'\cos\theta)^2)} \quad (1)$$

where, variable a is the axis scaling parameter of the transformation. The rotation variable θ controls the orientation and has a critical importance on finding the appropriate basis function that fits the corresponding lobe of the UAHS. Figure 6 shows the top and side views of the Gaussian basis functions which have the same a and ε parameters, but different θ parameter values.

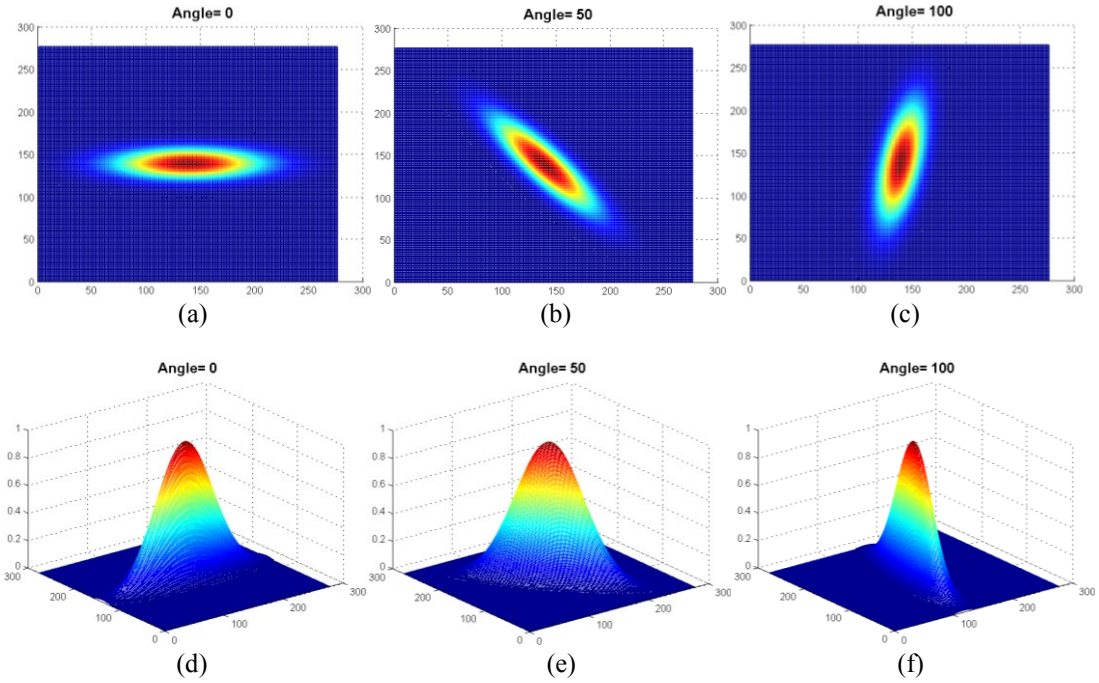

Figure 6 2-D Gaussian functions with respect to different angles (a)-(c) Top view (d)-(f) Side view.

Let us denote our final approximated UAHS as $UAHS(x,y)$ which is formed by combining all approximating Gaussian basis functions in an additive manner. However, before combining the suitable Gaussian basis functions, the best rotation angle among all possible choices of angles must be determined in an iterative manner. Here, each iteration corresponds to a different scale. Iterations start from the largest scale value and continue until the smallest scale value in a hierarchical manner. In our simulations, we used 8 different scale values. Thus, denoting the number of iterations by N, we have $N = 8$. For each scale, θ is varied from 0 up to a maximum of 170 degrees with an increment of 10 degrees. Thus, $\theta = \{0,10,\ldots,170\}$ defines the vector of rotations. Denoting the length of the vector, θ, by M, we have M=18. $Corr\{.\}$ is defined as the 2-D correlation operation between Gaussian basis function, $g_{a_i,\theta_j}(x',y')$, and the UAHS which is represented by *UAHS(x,y)*. For a fixed scale, the correlation is calculated for different rotations as:

$$\mathrm{Corr}_j = Corr\left\{g_{a_i,\theta_j}(x',y'), UAHS(x,y)\right\} \quad (2)$$

In Equation 3, we represent the best rotation angle as $\hat{\theta}$ which corresponds to the maximum correlation between UAHS and Gaussian basis functions.

$$\hat{\theta}=\arg\max_{\theta_j}\left(Corr\left\{g_{a_i,\theta_j}(x',y'),UAHS(x,y)\right\}\right)_{j=1}^{M} \tag{3}$$

We can express our approximated $UAHS(x,y)$ as a weighted summation of the rotated and axis scaled Gaussian basis functions, $g_{a_i,\theta_j}(x',y')$.

$$UAHS(x,y)=\sum_{i=1}^{N}\sum_{j=1}^{M}w_j g_{a_i,\theta_j}(x',y') \tag{4}$$

where $w_j=\begin{cases}1\ ; & \text{max correlation for scale } a_i \text{ among all possible } \theta_j \text{ angles}\\ 0\ ; & \text{for the rest of the } \theta_j \text{ angles}\end{cases}$

After approximating the UAHS, a method should be used to threshold the approximated UAHS by determining the two valleys so that upper and lower thresholds can be assigned correctly. Our main goal is to determine the two threshold values which correspond to the valleys on the left and right sides of the corresponding lobe of the organ of interest. As stated before, the main idea behind the Gaussian modeling is to find the basis functions that best fit the desired lobes and then to determine a threshold range to express the region of interest in the UAHS. Thus, after the Gaussian fitting step, as seen in Figure 7.a, the gray levels which belong to the organ of interest are grouped together. The center of the group is indicated by the mean of the gray levels, which are obtained via points through which the spline passes. The points, at which the tail of each Gaussian becomes zero, indicate the threshold range. As seen in Figure 7.b, a varying threshold range can be obtained using the Gaussian bases which are found by the multi-scale hierarchical model.

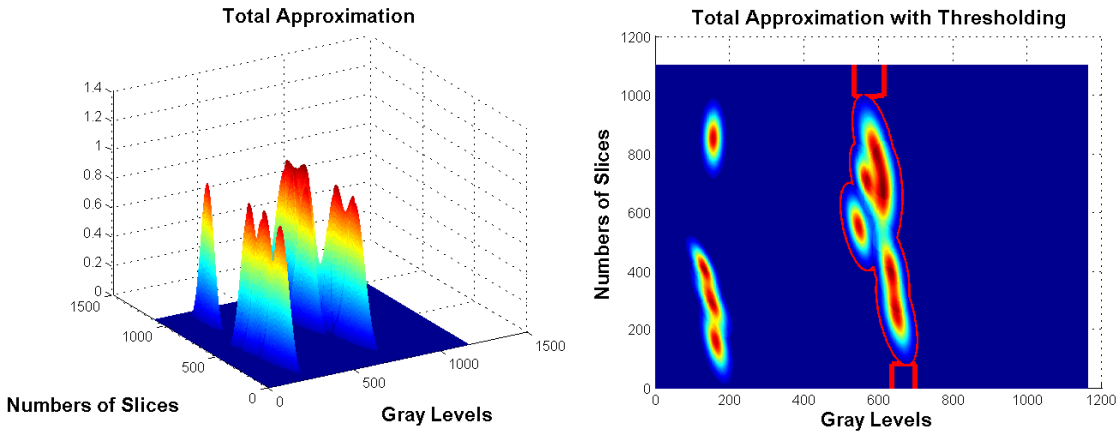

(a) (b)

Figure 7. (a) The resultant approximating Gaussian functions (b) Top view of the resultant approximation of Gaussian functions with a varying threshold range represented by red lines.

5. Application and Results

The developed method is evaluated using well established segmentation metrics including the area error rate (AER), which is defined as the area difference between the region segmented by the algorithm and the region segmented manually [21]. Volumetric overlap error (VOE) is similar to AER criterion where, 0 indicates perfect segmentation with no limitation for any upper bound [22]. Besides the difference in volume values, conformational characteristics of the obtained segmentation results are also important. For this purpose, Symmetric Surface Distance (SSD) metrics are also used for performance evaluations [22]. SSD allows the comparison of segmented 3-D organ with the reference 3-D organ by using surface voxels of a 3-D object. The surface voxels are defined according to at least one voxel that does not belong to the object in 18 possible neighboring. For each surface voxel in the reference organ, the distance to the surface voxel in the segmented organ is calculated according to the

Euclidean Distance Metric via different formulations that produce Average SSD (ASSD), Maximum SSD (MSSD), and RMS SSD (RSSD).

Some visual examples of the results are given in Figure 8 and calculated metrics for all the data sets are given in Table 1. Red pixels show True Positive pixels after the thresholding process. This means that the red pixels are classified as the organ of interest and these pixels are actual organ pixels. Therefore, it can be stated that by using Gaussian approximations and the thresholding process, the segmentation of the organ is accomplished substantially. Green pixels of the images represent the organ pixels which are not found by our algorithm. Finally, blue pixels are the pixels which belong to the unwanted pixels/neighboring tissues but are found as belonging to the organ of interest by our algorithm. Observing Figure 8, it can be stated that using the coarse approximation at the first and last slices is not enough for segmentation. In contrast to the first and last slices, in the middle of the image series our algorithm performs better.

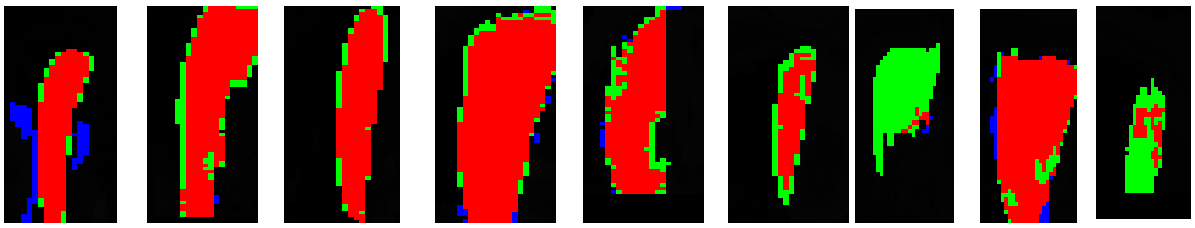

Figure 8 (From left to right) MPR images belonging to T1 WATS with slice numbers 3-11-21. T1-DUAL with slice numbers 12-18-24 and THRIVE with slice numbers 2-10-22.

The results show that the proposed approach can provide acceptable initial classification results by approximating the lobes of UAHS using proposed GMM strategy (i.e. see the first three rows of Table 1). On the other hand, these results must be enhanced for obtaining clinically usable visualizations. In this study, the finer classification steps include binary morphological operations and region growing using initial coarse classification results. The last three rows of Table 1 show that post-processing operations can significantly improve the results, since the initial model obtained by GMM is satisfactory. Future work could include using statistical shape models which would be initialized by the proposed GMM strategy.

Table 1. Comparison of the average metric results of all sequences before and after region growing.

	Dataset	***ASSD***	***RSSD***	***MSSD***	***AHO***	***VHO***
Without Post-Processing	**T1 DUAL**	3.69	6.72	34.30	53.89	44.69
	T1 WATS	6.95	11.37	46.47	54.04	52.46
	THRIVE	6.13	10.22	42.60	42.82	44.06
With Post-Processing ***(Region Growing)***	**T1 DUAL**	3.88	6.84	35.21	59.93	42.03
	T1 WATS	1.73	2.61	18.75	33.61	28.70
	THRIVE	2.97	3.97	17.69	29.62	28.51

Acknowledgment
This study is supported by The Scientific and Technological Research Council of Turkey (TÜBİTAK) under grant number EEEAG 112E032.

References

[1] Fischer, F., Selver, M.A., Hillen, W., Güzeliş, C, Integrating Segmentation Methods from Different Tools into a Visualization Program Using an Object Based Plug-In Interface, IEEE Transactions on Information Technology in Biomedicine, Vol. 14(4), 923-934, 2010.

[2] R. A. Drebin, L. Carpenter, and P. Hanrahan. Volume rendering, In Proceedings of ACM Siggraph 1988, pages 65–74, 1988.
[3] H. Pfister, B. Lorensen, C. Bajaj, G. Kindlmann, W. Schroeder, and R. Machiraju, The Transfer Function Bake-Off, In Proceedings of IEEE Visualization 2000, 523-526.
[4] F. Shiaofen, B. Tom, and T. Mihran, Image-Based Transfer Function Design for Data Exploration in Volume Visualization, In Proceedings of IEEE Visualization 1998, 319-326.
[5] A. Konig, and E. Gröller, Mastering Transfer Function Specification by Using VolumePro Technology, In Proceedings of Computer Graphics'01, vol. 17, 279-286, 2001.
[6] J. Marks, B. Andalman, P.A. Beardsley, and H. Pfister, Design Galleries: A General Approach to Setting Parameters for Computer Graphics and Animation. SIGGRAPH, (1997) 389-400.
[7] F. Shiaofen, B. Tom, and T. Mihran, Image-Based Transfer Function Design for Data Exploration in Volume Visualization, In Proceedings of IEEE Visualization 1998, 319-326.
[8] Liang Zhou, Hansen, C., Transfer function design based on user selected samples for intuitive multivariate volume exploration, Visualization Symposium IEEE Pacific, pp. 73 – 80, 2013.
[9] C. L. Bajaj, V. Pascucci, D. R. Schikore, The Contour Spectrum, IEEE Visualization, 1997, 167-173.
[10] G. Kindlmann, and J. W. Durkin, Semi-Automatic Generation of Transfer Functions for Direct Volume Rendering, In Proceedings of IEEE Visualization 1998, 79-86.
[11] I. Fujishiro, T. Azuma, and Y. Takeshima, Automating Transfer Function Design for Comprehensible Volume Rendering Based on 3D Field Topology Analysis, In Proc. of IEEE Visualization'98, 467-470.
[12] T. He, L. Hong, A. Kaufman and H. Pfister, Generation of Transfer Functions with Stochastic Search Techniques, In Proceedings of IEEE Visualization 1996, 227-234.
[13] Jesus J. Caban, Penny Rheingans, "Texture-based Transfer Functions for Direct Volume Rendering," IEEE Transactions on Visualization and Computer Graphics, vol. 14(6), 1364-1371, Nov./Dec. 2008.
[14] Y. Sato, C.F. Westin, A. Bhalerao, S. Nakajima, N. Shiraga, S. Tamura, and R. Kikinis, "Tissue Classification Based on 3D Local Intensity Structures for Volume Rendering", IEEE Trans. On Visualization and Computer Graphics, Vol.6, No.2, pp. 160-180, 2000.
[15] C. Rezk Salama, M. Keller, P. Kohlmann, High-Level User Interfaces for Transfer Function Design with Semantics, IEEE Transactions on Visualization and Computer Graphics, Vol. 12(5), 1021 – 1028, 2006.
[16] J. Kniss, G. Kindlmann, C. Hansen, Interactive Volume Rendering Using Multi-Dimensional Transfer Functions and Direct Manipulation Widget, Visualization 2001, 255-262.
[17] Eric B. Lum, James Shearer, Kwan-Liu Ma: Interactive multi-scale exploration for volume classification, The Visual Computer, vol. 22(9-11): 622-630 (2006)
[18] J. Kniss, G. Kindlmann, and C. Hansen, Multi-Dimensional Transfer Functions for Interactive Volume Rendering, IEEE Transactions on Visualization and Computer Graphics, vol. 8(3), 270-285, (2002).
[19] Fan-Yin Tzeng, Eric B. Lum, and Kwan-Liu Ma: An Intelligent System Approach to Higher-Dimensional Classification of Volume Data. IEEE Trans. On Vis. and Computer Graphics 11(3): 273-284 (2005).
[20] P. Rautek, S. Bruckner, and M. E. Groller, Semantic Layers for Illustrative Volume Rendering, IEEE Transactions on Visualization and Computer Graphics, Volume 13, Issue 6, Page(s):1336 – 1343, 2007.
[21] Seo, K. S., Ludeman, L. C., Park, S. J., & Park, J. A. (2004). Efficient liver segmentation based on the spine. Lecture Notes in Computer Science, 3261, 400-409.
[22] Ginneken, B. V., Heiman, T., & Styner, M. (2007). 3-D segmentation in the clinic: A grand challenge. MICCAI Workshop Proceedings, 7-15.
[23] C. Westbrook, Handbook of MRI technique. (3rd edt.). Oxford, United Kingdom: Wiley-Blackwell, 2008